Asian Journal of Chemistry; Vol. 25, No. 16 (2013), 8953-8956

ASIAN JOURNAL OF CHEMISTRY

http://dx.doi.org/10.14233/ajchem.2013.14929A

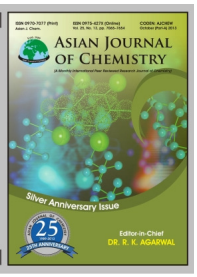

Preparation and Optical Properties of SPION/$SrMoO_4$:Er^{3+}, Yb^{3+} Composites *via* Cyclic Microwave-Assisted Metathetic Route

CHANG SUNG LIM

Department of Advanced Materials Science & Engineering, Hanseo University, Seosan 356-706, Republic of Korea

Corresponding author: Tel/Fax: +82 41 6601445; E-mail: cslim@hanseo.ac.kr

(*Received*: 8 December 2012; *Accepted*: 11 September 2013) AJC-14089

Er^{3+}/Yb^{3+} co-doped $SrMoO_4$ ($SrMoO_4$:Er^{3+}/$Yb3^{+)}$ composites with superparamagnetic iron oxide nanoparticles (SPIONs) incorporated were successfully synthesized by a cyclic microwave-assisted metathetic method, followed by heat-treatment. The microstructure exhibited well-defined and homogeneous morphology with $SrMoO_4$:Er^{3+}/Yb^{3+} particle sizes of 1-2 μm and Fe_3O_4 particle sizes of 0.1-0.5 μm. The Fe_3O_4 particles were self-preferentially crystallized and immobilized on the surface of $SrMoO_4$:Er^{3+}/Yb^{3+} particles. The synthesized SPIONs/$SrMoO_4$:Er^{3+}, Yb^{3+} composites were characterized by X-ray diffraction, scanning electron microscopy and energy-dispersive X-ray spectroscopy. Optical properties were examined using photoluminescence emission data and Raman spectroscopy.

Key Words: Fe_3O_4, $SrMoO_4$:Er^{3+}/Yb^{3+}, Cyclic microwave-assisted metathetic synthesis, Photoluminesecnce, Raman spectroscopy.

INTRODUCTION

Magnetic nanoparticles are a class of nanoparticles that can be manipulated under the influence of an external magnetic field. Magnetic nanoparticles are commonly composed of magnetic elements such as iron, nickel, cobalt and their oxides. Superparamagnetic iron oxide nanoparticles (SPIONs) are superior to other metal oxide nanoparticles for their biocompatabilties and stabilities, because they are the most commonly employed magnetic nanoparticles in biological applications as dual-modality imaging probes in fluorescence detection, enhanced magnetic resonance imaging, selective magnetic separation, information storage in biotechnology, medicine and quality inspection[1]. Recently, bifunctional Fe_3O_4 incorporated photoluminescent composites have attracted great attention which provide novel characteristics *via* the integration of fluorescent and magnetic properties, offering new potential in a wide range of applications in biomedical systems, such as targeted drugs, diagnostics, therapeutics and bio-imaging[2,3]. Particles of rare-earth-doped $SrMoO_4$, which is at type of metallic molybdate compound with a schleelite-type structure and lattice parameters a = b = 5.3796 Å and c = 11.9897 Å[4-6], are relatively stable in air and have stable physical and chemical properties, low excitation threshold energy and low-cost productivity.

Several processes have been developed to increase the applications of rare-earth-doped metal molybdates prepared using a range of processes, including solid-state reactions[7-11], co-precipitation[12], the sol-gel method[13], the hydrothermal method[14-16], the Pechini method[17], the solvothermal route[18] and the microwave-assisted hydrothermal method[19]. For practical application of photoluminescence in such products as lasers, three-dimensional displays, light emitting devices and biological detectors, features such as homogeneous particle size distribution and morphology need to be well defined. Compared with the usual methods, microwave synthesis has the advantages of short reaction time, small-size particles, narrow particle size distribution and high purity for preparing polycrystalline samples. Microwave energy is delivered directly to the material by molecular interactions under an electric field. This makes it possible to rapidly and uniformly heat thick materials. Cyclic microwave-assisted metathetic (MAM) synthesis of materials is a simple and cost-effective method that provides high yield with easy scale-up and is emerging as a viable alternative approach for the synthesis of high-quality novel inorganic materials in short time periods[4,5,20]. However, the cyclic microwave-assisted metathetic synthesis of the SPION/$SrMoO_4$:Er^{3+}/Yb^{3+} composites and their optical properties have not been reported. Understanding the precise nature of the SPION/$SrMoO_4$:Er^{3+}, Yb^{3+} composites is required for a wide range of applications.

In this study, SPIONs incorporated Er^{3+}-doped $SrMoO_4$ ($SrMoO_4$:Er^{3+}) and Er^{3+}/Yb^{3+} co-doped $SrMoO_4$ ($SrMoO_4$:Er^{3+}/Yb^{3+}) composites were synthesized by the cyclic microwave-assisted metathetic method, followed by heat-treatment. The synthesized SPIONs/$SrMoO_4$:Er^{3+} and Fe_3O_4/$SrMoO_4$:Er^{3+}, Yb^{3+} composites were characterized by X-ray diffraction (XRD),

scanning electron microscopy and energy-dispersive X-ray spectroscopy. Optical properties were examined by using photoluminescence emission data and Raman spectroscopy.

EXPERIMENTAL

Appropriate stoichiometric amounts of $SrCl_2·2H_2O$, $ErCl_3·6H_2O$, $YbCl_3·6H_2O$, $Na_2MoO_4·2H_2O$, 5-nm-sized Fe_3O_4 nanoparticles and ethylene glycol of analytic reagent grade were used to prepare the $Fe_3O_4/SrMoO_4:Er^{3+}$, $Fe_3O_4/SrMoO_4:Er^{3+}$, Yb^{3+} and $SrMoO_4:Er^{3+}$, Yb^{3+} compounds. To prepare $Fe_3O_4/SrMoO_4:Er^3$, 0.95 mol % $SrCl_2·2H_2O$ with 0.05 mol % $ErCl_3·6H_2O$ and 1 mol % $Na_2MoO_4·2H_2O$ with 0.5 mol % Fe_3O_4 were dissolved in 30 mL ethylene glycol, respectively. For preparation of $Fe_3O_4/SrMoO_4:Er^{3+}$, Yb^{3+}, 0.9 mol % $SrCl_2·2H_2O$ with 0.05 mol % $ErCl_3·6H_2O$ and 0.05 mol % $YbCl_3·6H_2O$ and 1 mol % $Na_2MoO_4·2H_2O$ with 0.5 mol % Fe_3O_4 were dissolved in 30 mL ethylene glycol, respectively. But to prepare $SrMoO_4:Er^{3+}$, Yb^{3+}, 0.9 mol % $SrCl_2·2H_2O$ with 0.05 mol % $ErCl_3·6H_2O$ and 0.05 mol % $YbCl_3·6H_2O$ and 1 mol % $Na_2MoO_4·2H_2O$ were dissolved in 30 mL ethylene glycol, respectively.

The solutions were mixed and adjusted to pH 9.5 using NaOH. The aqueous solutions were stirred at room temperature. The mixtures were transferred into 120 mL Teflon vessels. Each Teflon vessel was placed into a microwave oven operating at a frequency of 2.45 GHz with a maximum output power of 1250 W for 23 min. The working cycle of the microwave-assisted metathetic reaction was controlled very precisely between 30 sec on and 30 sec off for 8 min, followed by further treatment of 30 sec on and 60 sec off for 15 min. The ethylene glycol was evaporated slowly at its boiling point. Ethylene glycol is a polar solvent at its boiling point of 197 ºC and a good candidate for the microwave process. When ethylene glycol is used as the solvent, reactions proceed at the boiling point temperature. The microwave radiation is supplied to the ethylene glycol and the components dissolving in the ethylene glycol couple with each other under the radiation. When a large amount of microwave radiation is supplied to the ethylene glycol, the charged particles vibrate interdependently within the electric field. The resulting samples were treated with ultrasonic radiation and washed many times with hot distilled water. The white precipitates were collected and dried at 100 ºC in a drying oven. The final products were heat-treated at 600 ºC for 3 h.

The phase of the composites after the cyclic microwave-assisted metathetic reaction and heat-treatment was identified using XRD (D/MAX 2200, Rigaku, Japan). The microstructures and surface morphologies of the $Fe_3O_4/SrMoO_4:Er^{3+}$ and $Fe_3O_4/SrMoO_4:Er^{3+}$, Yb^{3+} composites were observed using SEM/EDS (JSM-5600, JEOL, Japan). Their photoluminescence spectra were recorded using a spectrophotometer (Perkin Elmer LS55, UK) at room temperature. Raman spectroscopy measurements were performed using a LabRam HR (Jobin-Yvon, France). The 514.5-nm line of an Ar-ion laser was used as an excitation source and the power on the samples was kept at 0.5 mW.

RESULTS AND DISCUSSION

Fig. 1 shows the XRD pattern of the synthesized $Fe_3O_4/SrMoO_4:Er^{3+}$, Yb^{3+} composites. The diffraction peaks marked with*are indexed to Fe_3O_4. All of the XRD peaks could be assigned to the tetragonal-phase $SrMoO_4$ with a scheelite-type structure and Fe_3O_4, which were in good agreement with the crystallographic data of $SrMoO_4$ (JCPDS 08-0482) and Fe_3O_4 (JCPDS 19-0629). This means that the $Fe_3O_4/SrMoO_4:Er^{3+}$, Yb^{3+} composites can be prepared using the cyclic microwave-assisted metathetic route. Post heat-treatment plays an important role in forming well-defined crystallized morphology. To achieve such morphology, the $Fe_3O_4/SrMoO_4:Er^{3+}$ and $Fe_3O_4/SrMoO_4:Er^{3+}$,Yb^{3+} composites need to be heat treated at 600 ºC for 3 h. This suggests that the cyclic microwave-assisted metathetic route is suitable for growing $Fe_3O_4/SrMoO_4:Er^{3+}$ and $Fe_3O_4/SrMoO_4:Er^{3+}$,Yb^3 composites and for developing the strongest intensity peaks at the (112), (204) and (312) planes, which are the major peaks of $SrMoO_4$[4-6].

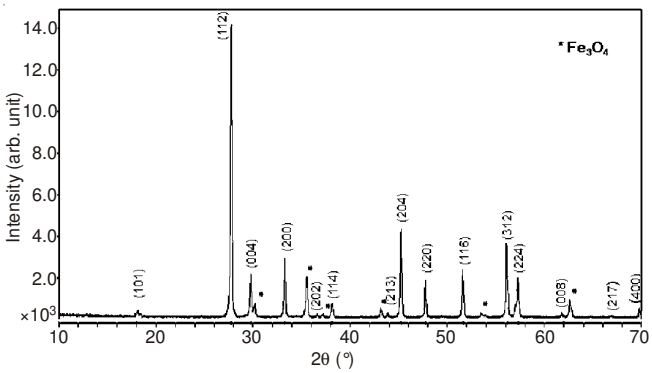

Fig. 1. XRD pattern of the synthesized SPION/$SrMoO_4:Er^{3+}$,Yb^{3+} composites

Fig. 2 shows the SEM image of the synthesized $Fe_3O_4/SrMoO_4:Er^{3+}$,Yb^{3+} composites. The as-synthesized sample has well-defined and homogeneous morphology with $SrMoO_4:Er^{3+}/Yb^{3+}$ particle sizes of 1-2 μm and Fe_3O_4 particle sizes of 0.1-0.5 μm, respectively. The Fe_3O_4 particles were self-preferentially crystallized and immobilized on the surface of $SrMoO_4:Er^{3+}/Yb^{3+}$ particles. Fig. 3 shows (a) an EDS pattern, (b) quantitative compositions, (c) quantitative results and (d) an SEM image of the synthesized $Fe_3O_4/SrMoO_4:Er^{3+}$, Yb^{3+} composites. The EDS pattern shows that the $Fe_3O_4/SrMoO_4:Er^{3+}$, Yb^{3+} composites are composed of Fe, Sr, Mo, O, Er

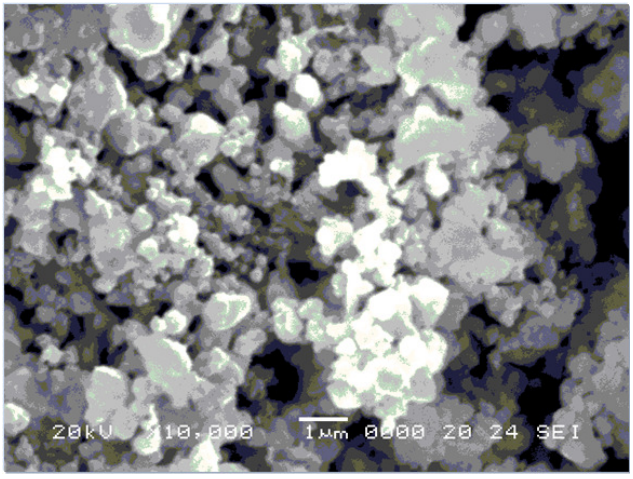

Fig. 2. SEM image of the synthesized SPION/$SrMoO_4:Er^{3+}$, Yb^{3+} composites

and Yb in Fig. 3(a) and identified as the quantitative compositions in Fig. 3(b). The EDS pattern and quantitative compositions in Figs. 3 (a, b) could be assigned to the Fe_3O_4/$SrMoO_4$:Er^{3+}, Yb^{3+} composites. This means that the $SrMoO_4$:Er^{3+}, Yb^{3+} composites with Fe_3O_4 nanoparticles incorporated can be successfully synthesized using this cyclic microwave-assisted metathetic method. Cyclic microwave-assisted metathetic reactions, such as $SrCl_2 + Na_2MoO_4 \rightarrow SrMoO_4 + 2NaCl$, involve the exchange of atomic/ionic species, in which the driving force is the exothermic reaction accompanying the formation of NaCl[4,20]. Cyclic microwave-assisted metathetic reactions occur so rapidly that the exothermic reaction is essentially used to heat up the solid products. The cyclic microwave-assisted metathetic reactions provide a convenient route for the synthesis of Fe_3O_4/$SrMoO_4$:Er^{3+} and Fe_3O_4/$SrMoO_4$:Er^{3+},Yb^{3+} composites. The cyclic microwave-assisted metathetic route[20] provides the exothermic energy to synthesize the bulk of the material uniformly, so that fine particles with controlled morphology can be fabricated in an environmentally friendly manner without the generation of solvent waste. Fe_3O_4/$SrMoO_4$:Er^{3+} and Fe_3O_4/$SrMoO_4$:Er^{3+}, Yb^{3+} composites were heated rapidly and uniformLy by the cyclic microwave-assisted metathetic route. This makes the method a simple and cost-effective and able to provide high yields with easy scale-up, as a viable alternative for the rapid synthesis of Fe_3O_4/$SrMoO_4$:Er^{3+} and Fe_3O_4/$SrMoO_4$:Er^{3+}, Yb^{3+} composites.

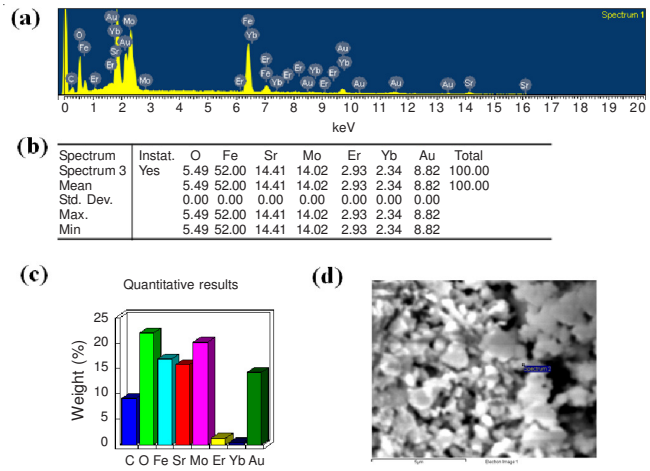

Spectrum	Instat.	O	Fe	Sr	Mo	Er	Yb	Au	Total
Spectrum 3	Yes	5.49	52.00	14.41	14.02	2.93	2.34	8.82	100.00
Mean		5.49	52.00	14.41	14.02	2.93	2.34	8.82	100.00
Std. Dev.		0.00	0.00	0.00	0.00	0.00	0.00	0.00	
Max.		5.49	52.00	14.41	14.02	2.93	2.34	8.82	
Min		5.49	52.00	14.41	14.02	2.93	2.34	8.82	

Fig. 3. A (a) EDS pattern, (b) quantitative compositions, (c) quantitative results and (d) a SEM image of the synthesized SPION/$SrMoO_4$:Er^{3+}, Yb^{3+} composites

Fig. 4 shows the photoluminescence emission spectra of the synthesized (a) Fe_3O_4/$SrMoO_4$:Er^{3+} and (b) Fe_3O_4/$SrMoO_4$:Er^{3+}, Yb^{3+} composites excited at 250 nm at room temperature. The emission spectrum of metal molybdates is due mainly to charge-transfer transitions within the $[MoO_4]^{2-}$ complex[21,22]. With excitation at 250 nm, the Fe_3O_4/$SrMoO_4$:Er^{3+} and Fe_3O_4/$SrMoO_4$:Er^{3+}, Yb^{3+} composites exhibit photoluminescence emission in the blue wavelength range of 370-430 nm. The photoluminescence intensity of the (b) Fe_3O_4/$SrMoO_4$:Er^{3+}, Yb^{3} is slightly stronger than that of the (a) Fe_3O_4/$SrMoO_4$:Er^{3+}. The doping amounts of Er^{3+}/Yb^{3+} have an effect on the photoluminescence intensity. This suggests that the doping amounts play an important role in improving the luminescent efficiency. The photoluminescence intensity of energy-conversion materials depends strongly on not only the particle shape and distribution but also the doping amounts. Generally, for similar morphological samples, homogenized particles are favourable for the luminescent characteristics, because of the lesser contamination or fewer dead layers on the surface of the energy-conversion materials. The five narrow shoulders in the emission spectra at approximately 480, 510, 530, 540 and 545 nm are believed to be due to a defect structure23. Such peaks, producing a spread-eagle shape of the blue emission, can be explained by the influence of the Jahn-Teller effect[24,25] on the degenerated excited state of the $[MoO_4]^{2-}$ tetrahedron. Generally, the presence of Gaussian components indicates that the electronic levels corresponding to the relaxed excited state of an emission centre belong to a degenerate excited state influenced by some perturbation, *e.g.* a local low symmetry crystal field[23]. The Jahn-Teller splitting effect essentially determines the emission shape of the $MMoO_4$ (M= Ca, Ba, Sr) particles. The additional emission bands can be explained by the existence of a Frenkel defect structure (oxygen ions shifted to the inter-position with the simultaneous creation of vacancies)[26].

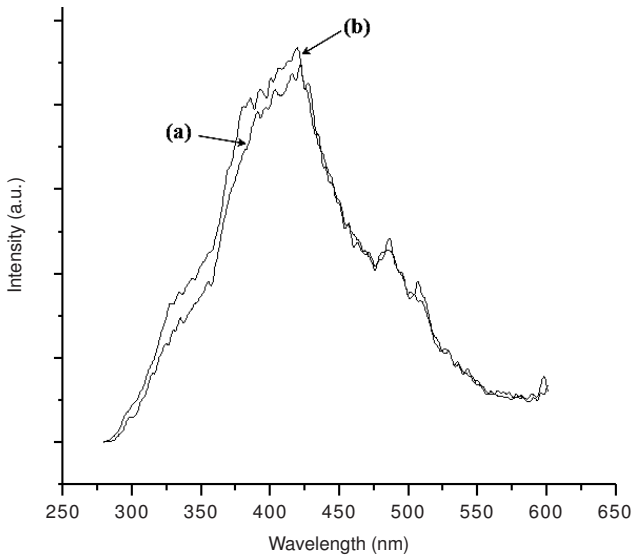

Fig. 4. Photoluminescence emission spectra of the synthesized (a) SPION/$SrMoO_4$:Er^{3+} and (b) SPION/$SrMoO_4$:Er^{3+}, Yb^{3+} composites excited at 250 nm at room temperature

Fig. 5 shows Raman spectra of the synthesized (a) $SrMoO_4$:Er^{3+}, Yb^{3+} (SMO:ErYb) particles and (b) Fe_3O_4/$SrMoO_4$:Er^{3+}, Yb^{3+} (F-SMO:ErYb) composites excited by the 514.5-nm line of an Ar-ion laser at 0.5 mW. The Raman spectra show that the peak positions and intensities are the same. The internal modes the synthesized (a) $SrMoO_4$:Er^{3+}, Yb^{3+} (SMO:ErYb) particles and (b) Fe_3O_4/$SrMoO_4$:Er^{3+}, Yb^{3+} (F-SMO:ErYb) composites were detected as $\nu_1(A_g)$, $\nu_3(B_g)$, $\nu_3(E_g)$, $\nu_4(E_g)$, $\nu_4(B_g)$ and $\nu_2(B_g)$ vibrations at 887, 844, 796, 380, 357 and 338 cm^{-1}, respectively. A free rotation mode was detected at 180 cm^{-1} and the external modes were localized at 137 and 111 cm^{-1}. The well-resolved sharp peaks for the $SrMoO_4$ particles indicate the high crystallization of the synthesized particles. The internal vibration mode frequencies are dependent on the lattice parameters and the degree of the partially

covalent bond between the cation and molecular ionic group $[MoO_4]^{2-}$. The Raman spectra of the synthesized (a) $SrMoO_4$:Er^{3+}, Yb^{3+} (SMO:ErYb) particles and (b) Fe_3O_4/$SrMoO_4$:Er^{3+}, Yb^{3+} (F-SMO:ErYb) composites indicate the detection of additional strong peaks at both higher frequencies (556, 520, 458 and 403 cm^{-1}) and lower frequencies (295, 253 and 224 cm^{-1}). Atuchin *et al.*[27-29] could consider that the very strong and strange effect in the Ln-doped crystalline samples may be generated by the disorder of the MoO_4 groups with the incorporation of the Ln element into the crystal lattice or by a new phase formation. It is noted that the Fe_3O_4 particles have no influence on the Raman spectra, while the doping ion of Er^{3+}/Yb^{3+} can influence the Raman spectra. The Raman spectra proved that the doping ion of Er^{3+}/Yb^{3+} can influence the structure of the host materials.

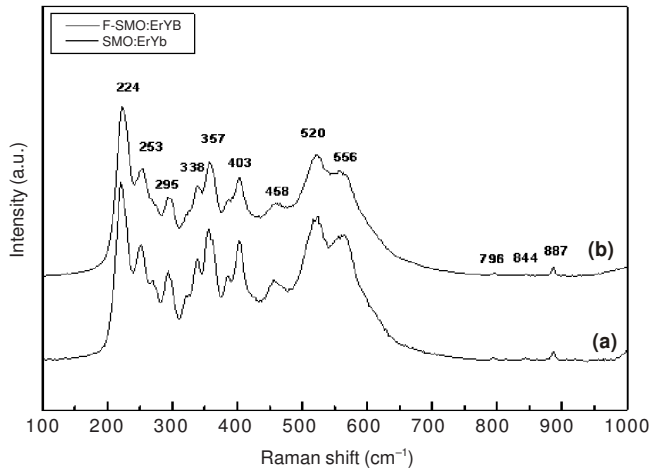

Fig. 5. Raman spectra of the synthesized (a) $SrMoO_4$:Er^{3+} (SMO:ErYb) particles and (b) SPION/$SrMoO_4$:Er^{3+}, Yb^{3+} (F-SMO:ErYb) composites excited by the 514.5-nm line of an Ar-ion laser at 0.5 mW on the samples

Conclusion

SPION/$SrMoO_4$:Er^{3+}, Yb^{3+} composites were successfully synthesized by a cyclic microwave-assisted metathetic method. The microstructure exhibited well-defined and homogeneous morphology with $SrMoO_4$:Er^{3+}/Yb^{3+} particle sizes of 1-2 μm and Fe_3O_4 particle sizes of 0.1-0.5 μm. The Fe_3O_4 particles were self-preferentially crystallized and immobilized on the surface of $SrMoO_4$:Er^{3+}/Yb^{3+} particles. With excitation at 250 nm, the SPION/$SrMoO_4$:Er^{3+} and Fe_3O_4/$SrMoO_4$:Er^{3+}, Yb^{3+} compo-sites exhibit photoluminescence emission in the blue wavelength range of 370-430 nm. The Raman spectra of the synthesized $SrMoO_4$:Er^{3+}, Yb^{3+} (SMO:ErYb) particles and SPION/$SrMoO_4$:Er^{3+}, Yb^{3+} (F-SMO:ErYb) composites indicate the detection of additional strong peaks at both higher frequencies (556, 520, 458 and 403 cm^{-1}) and lower frequencies (295, 253 and 224 cm^{-1}). The Fe_3O_4 particles have no influence on the Raman spectra, while the doping ion of Er^{3+}/Yb^{3+} can influence the Raman spectra. The Raman spectra proved that the doping ion of Er^{3+}/Yb^{3+} can influence the structure of the host materials.

ACKNOWLEDGEMENTS

This study was supported by Research Program through the Campus Research Foundation funded by Hanseo University in 2013 (131Egong06).

REFERENCES

1. D. Liu, L. Tong, J. Shi and H. Yang, *J. Alloys Comp.*, **512**, 361 (2012).
2. L. Liu, L. Xiao and H.Y. Zhu, *Chem. Phys. Lett.*, **539-540**, 112 (2012).
3. Q. Wang, X. Yang, L. Yu and H. Yang, *J. Alloys Comp.*, **509**, 9098 (2011).
4. J.C. Sczancoski, L.S. Cavalante, M.R. Joya, J.A. Varela, P.S. Pizani and E. Longo, *Chem. Eng. J.*, **140**, 632 (2008).
5. T. Thongtem, S. Kungwankunakorn, B. Kuntalue, A. Phuruangrat and S. Thongtem, *J. Alloys Comp.*, **506**, 475 (2010).
6. T. Thongtem, A. Phuruangrat and S. Thongtem, *J. Nanopart. Res.*, **12**, 2287 (2010).
7. C.S. Lim, *Asian J. Chem.*, **24**, 3323 (2012).
8. L.Y. Zhou, J.S. Wei, F.Z. Gong, J.L. Huang and L.H. Yi, *J. Solid State Chem.*, **181**, 1337 (2008).
9. J. Liu, H. Lian and C. Shi, *Optical Mater.*, **29**, 1591 (2007).
10. X. Li, Z. Yang, L. Guan, J. Guo, Y. Wang and Q. Guo, *J. Alloys Comps.*, **478**, 684 (2009).
11. D. Gao, Y. Li, X. Lai, Y. Wei, J. Bi, Y. Li and M. Liu, *Mater. Chem. Phys.*, **126**, 391 (2011).
12. Y. Yang, X. Li, W. Feng, W. Yang, W. Li and C. Tao, *J. Alloys Comp.*, **509**, 845 (2011).
13. F.B. Cao, L.S. Li, Y.W. Tian, Y.J. Chen and X.R. Wu, *Thin Solid Films*, **519**, 7971 (2011).
14. Y. Jin, J. Zhang, Z. Hao, X. Zhang and X.J. Wang, *J. Alloys Comp.*, **509**, L348 (2011).
15. F. Yu, J. Zuo, Z. Zhao, C. Jiang and Q. Yang, *Mater. Res. Bull.*, **46**, 1327 (2011).
16. F. Lei and B. Yan, *J. Sol. State Chem.*, **181**, 855 (2008).
17. Z.J. Zhang, H.H. Chen, X.X. Yang and J.T. Zhao, *Mater. Sci. Eng. B*, **145**, 34 (2007).
18. N. Niu, P. Yang, W. Wang, F. He, S. Gai, D. Wang and J. Lin, *Mater. Res. Bull.*, **46**, 333 (2011).
19. J. Zhang, X. Wang, X. Zhang, X. Zhao, X. Liu and L. Peng, *Inorg. Chem. Comm.*, **14**, 1723 (2011).
20. C.S. Lim, *Mater. Chem. Phys.*, **131**, 714 (2012).
21. D.A. Spassky, S.N. Ivanov, V.N. Kolobanov, V.V. Mikhailin, V.N. Zemskov, B.I. Zadneprovski and L.I. Potkin, *Radiat. Meas.*, **38**, 607 (2004).
22. G.Y. Hong, B.S. Jeon, Y.K. Yoo and J.S. Yoo, *J. Electrochem. Soc.*, **148**, H161 (2001).
23. K. Polak, M. Nikl, K. Nitsch, M. Kobayashi, M. Ishii, Y. Usuki and O. Jarolimek, *J. Luminescence*, **72-74**, 781 (1997).
24. Y. Toyozawa and M. Inoue, *J. Phys. Soc. Jpn.*, **21**, 1663 (1966).
25. E.G. Reut, *Izv. Akad. Nauk SSSR, Ser. Fiz.*, **43**, 1186 (1979).
26. V.B. Mikhailik, H. Kraus, D. Wahl and M.S. Mykhaylyk, *Phys. Status Solid B*, **242**, R17 (2005).
27. V.V. Atuchin, O.D. Chimitova, T.A. Gavrilova, M.S. Molokeev, S.J. Kim, N.V. Surovtsev and B.G. Bazarov, *J. Crystal. Growth*, **318**, 638 (2011).
28. V.V. Atuchin, V.G. Grossman, S.V. Adichtchev, N.V. Surovtsev, T.A. Gavrilova and B.G. Bazarov, *Opt. Mater.*, **34**, 812 (2012).
29. I.B. Troitskaia, T.A. Gavrilova, S.A. Gromilov, D.V. Sheglov, V.V. Auchin, R.S. Vemuri and C.V. Ramana, *Mater. Sci. Eng. B*, **174**, 159 (2010).